Flow velocities of the debris-covered Miyar Glacier, western Himalaya, India

Article *in* Geografiska Annaler Series A Physical Geography · December 2021

DOI: 10.1080/04353676.2021.2022355

Suresh Das
Jawaharlal Nehru University

Katie E Miles
Aberystwyth University

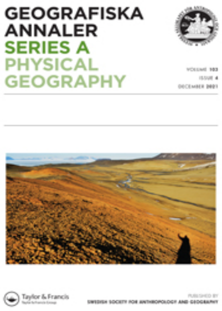

Geografiska Annaler: Series A, Physical Geography

ISSN: (Print) (Online) Journal homepage: https://www.tandfonline.com/loi/tgaa20

Flow velocities of the debris-covered Miyar Glacier, western Himalaya, India

Suresh Das, Milap Chand Sharma & Katie E. Miles

To cite this article: Suresh Das, Milap Chand Sharma & Katie E. Miles (2021): Flow velocities of the debris-covered Miyar Glacier, western Himalaya, India, Geografiska Annaler: Series A, Physical Geography, DOI: 10.1080/04353676.2021.2022355

To link to this article: https://doi.org/10.1080/04353676.2021.2022355

Published online: 30 Dec 2021.

GEOGRAFISKA ANNALER: SERIES A, PHYSICAL GEOGRAPHY
https://doi.org/10.1080/04353676.2021.2022355

Flow velocities of the debris-covered Miyar Glacier, western Himalaya, India

Suresh Das [a], Milap Chand Sharma [a] and Katie E. Miles [b]

[a]Centre for the Study of Regional Development (CSRD), Jawaharlal Nehru University, New Delhi, India; [b]Centre for Glaciology, Department of Geography and Earth Sciences, Aberystwyth University, Aberystwyth, UK

ABSTRACT

Spatiotemporal surface velocity measurements of the alpine valley type debris-covered Miyar Glacier of the Chandrabhaga (Chenab) basin, western Himalaya, were assessed based on the cross-correlation of Landsat images spanning nearly three decades (1992-2019). Long-term (1950-2015) temperature and precipitation trends were evaluated using Asian Precipitation Highly Resolved Observational Data Integration Towards Evaluation (APHRODITE) datasets. The mean velocity (1992-2019) of the Miyar Glacier is ~29 m/yr, with spatial patterns revealing that the debris-covered tongue is nearly stagnant (~5 m/yr) compared to the debris-free up-glacier zone (~35 m/yr). The transition zone from clean to debris-covered ice in the mid-ablation area shows the highest long-term mean velocities of ~60 m/yr during the observation period, likely resulting from a steep surface gradient and greater ice thickness than the other regions of this glacier. The slow-moving and nearly stagnant debris-covered area reveals the highest amount of surface lowering due to the expansion of supraglacial ponds. Miyar Glacier experiences summer speed-up of ~67–80% in seasonal velocity compared to winter, interpreted as a result from enhanced basal sliding during summer months due to warmer temperatures inputting more meltwater into the subsurface drainage system. Inter-annual velocity variations are greatest in the upper glacier, with higher velocities observed more frequently in recent decades. Future work should aim to elucidate the causes of this pattern, considering the overall rising air temperature trend in the western Himalaya.

ARTICLE HISTORY
Received 13 August 2021
Revised 6 December 2021
Accepted 9 December 2021

KEYWORDS
Glacier velocity; COSI-Corr; aphrodite; debris-covered ice; subglacial hydrology; himalaya

1. Introduction

Glaciers move or flow downhill in response to the gravitational forces generated by their mass (Nye 1952), through internal deformation of ice (Glen 1955), basal sliding (Weertman 1957), and/or subglacial deformation (Bindschadler 1983). The types of movement exhibited by a glacier are closely related to the temperature of the ice (Cuffey and Paterson 2010). For instance, basal sliding is more efficient in warm-based glaciers where water is available at the glacier's base and lubricates the rock/ice interface (Bindschadler 1983). Similarly, bed deformation is more effective beneath warm-based glaciers since the underlying unfrozen sediments will be saturated with water, reducing these materials' frictional strength (Benn and Evans 2010; Cuffey and Paterson 2010). For glacier movement dominated by internal deformation, the transverse glacier profile (velocity distribution across the glacier) exhibits a parabolic shape, with maximum velocities near the center of the valley that

CONTACT Suresh Das suresh41_ssf@jnu.ac.in Centre for the Study of Regional Development (CSRD), Jawaharlal Nehru University, New Delhi 110067, India
Supplemental data for this article can be accessed at https://doi.org/10.1080/04353676.2021.2022355

decrease towards valley walls. In contrast, glacier velocity dominated by basal motion shows a more flat (uniform) transverse velocity profile (Jiskoot 2011).

As a significant agent of landscape changes, glacier movement or stagnation is of notable interest to the geomorphologist (Watson and Quincey 2015). The implication of glacier movement includes reconstructing the past glacier extent (Benn and Evans 2010), assessing glacial lake formation due to recession (Shugar et al. 2020) and associated hazards (Westoby et al. 2014), and examining glacier morphology and dynamics due to surge events (Quincey et al. 2011; Bhambri et al. 2020) or stagnation and surface lowering of debris-covered glaciers (Thompson et al. 2016; Steiner et al. 2021). Velocity assessment of debris-covered glaciers is important due to their complex response to climate change (Watson and Quincey 2015; Miles et al. 2018). Debris-covered glaciers that are stagnating and losing mass primarily through surface lowering can be more prone to the development of supraglacial ponds, which can accelerate mass loss (Thompson et al. 2016; Miles et al. 2020; Steiner et al. 2021). Therefore, it can be assumed that the surface velocity has a significant impact on the health and sustenance of a glacier.

Ice velocity can be measured in the field by monitoring the position of stakes over time using dGPS measurements, which can be time consuming and is often infeasible for glaciers in the Himalaya due to rugged topography, harsh climate, and inaccessibility. As a result, field-based velocity studies commonly have sparse records on a spatial and temporal scale and measure point-based surface displacement, which cannot represent the entire glacier. Only a few studies have been published on stake-based surface velocity measurements in western (Wagnon et al. 2007a; Azam et al. 2014) and central Himalaya (Wagnon et al. 2013). In contrast, remote sensing-based measurements provide the opportunity to achieve extensive and near complete spatial coverage over a glacier even in the remotest areas in the Himalaya (Scherler et al. 2008; Copland et al. 2009; Dehecq et al. 2015; 2019). In the early twenty-first century, studies have been published on individual- or basin-scale glacier surface velocity estimations across the eastern (e.g. Tsutaki et al. 2018), central (e.g. Quincey et al. 2009; Nuimura et al. 2011), and western Himalaya (e.g. Scherler et al. 2008; Satyabala 2016; Shukla and Garg 2020) based on remote-sensing measurements. Globally available surface velocity maps from the Global Land Ice Velocity Extraction from Landsat (GoLIVE; Fahnestock et al. 2016; Dehecq et al. 2019) and the Inter-mission Time Series of Land Ice Velocity and Elevation (ITSLIVE; Scambos et al. 2016; Gardner et al. 2018) projects are available at very coarse resolution (> 300 m) but are thus less suited to small-scale studies in mountainous regions (Millan et al. 2019).

In the western Himalaya, most of the previous studies on surface velocity measurements are concentrated in the upper Chandra (Sahu and Gupta 2019; Patel et al. 2021) and Zanskar basin (Bhushan et al. 2018; Garg et al. 2021). In the upper Chandra basin, Bara Shigri, Chhota Shigri, Samudra Tapu, and Panchi Nala glaciers are the most studied in terms of surface velocity (Garg et al. 2017; Shukla and Garg 2019; Yellala et al. 2019; Patel et al. 2021). Recently, Das and Sharma (2021) presented surface velocity measurements for 33 glaciers in the adjacent Jankar Chhu watershed, Bhaga basin (a tributary of Chandrabhaga river). Miyar is one of the longest (~27 km) and largest (~84.2 km^2 in size in 2019) glacier in the Chandrabhaga basin, western Himalaya (Deswal et al. 2017). Comprehensive glaciological studies have not been carried out for the Miyar Glacier due to its inaccessibility and logistical difficulties. However, to the best of our knowledge, no studies have investigated surface velocity measurements of the Miyar Glacier. In this study, we present surface velocity measurements of the Miyar Glacier during the last three decades (1992-2020) based on the cross-correlation of Landsat images. In addition, the possible influence of several topographical factors and climatic conditions are highlighted to characterize the dynamic nature of surface velocity.

2. Study area

The Miyar basin extends between 32°42′36″ N and 33°15′24″ N, and 76°40′12″ E and 77°1′15″ E in the western Himalaya region, ranging in elevation from 2800 m to over 6500 m above sea level (a.s.l). This basin contains 92 glaciers (> 0.2 km^2 in size) of varying dimensions and types, of which Miyar is the largest, fed by several tributaries (Figure 1) (Saini et al. 2019). Miyar is a broad valley-type alpine debris-covered glacier. The Miyar river originates from this glacier, flowing into the Chandrabhaga (Chenab) river at Udaipur (32.72°N, 76.66° E) in the Lahaul-Spiti district of Himachal Pradesh, India (Deswal et al. 2017) (Figure 1b). The total area of the Miyar Glacier is 84.2 km^2 as in 2019, with nearly one-third (24.1 km^2; 28.6%) covered by debris. The maximum elevation of Miyar Glacier is ~6236 m a.s.l, and the present-day snout of the glacier terminates at ~4060 m a.s.l. The surface gradient is steepest in the upper glacier (> 25°) along the central flow line, while the debris-covered zone is low of gradient (< 5°). Numerous ice cliffs and supraglacial lakes characterize the debris-covered ablation zone of the Miyar Glacier (Figure 1c).

Climatically, the Lahaul region is located between the monsoon-dominated areas of the Pir Panjal to the south and the mid-latitude Westerlies-dominated arid regions to the north (Deswal et al. 2017). The basin is dominated by severe and long winters that last from September to May, with minimum temperatures of −15°C. However, during the summer months (May-September), temperatures can rise to 30°C (Deswal et al. 2017; Saini et al. 2019; Prakash et al. 2021). Miyar basin remains snow-covered for almost six months and receives an average snowfall of 120–400 cm/year (Deswal et al. 2017; Patel et al. 2018). The annual precipitation is dominated by the snowfall which is controlled by the mid-latitude Westerlies (Saini et al. 2019). The contemporary Equilibrium Line Altitude (ELA) lies between 4900 and 5200 m a.s.l (Deswal et al. 2017; Saini et al. 2019).

3. Data and methods

3.1. Field data

A limited number of field measurements have been made in the Miyar basin in recent years. Snout position of Miyar Glacier was mapped in 2013 using handheld GPS Garmin Etrex. Field photographs were taken to characterize the surface morphology at the snout (Figure 2a). A weather station was set up at Tingret village in 2015, which is 40 km downstream from the present-day snout (Figures 1b and 2b). A glaciological research station was established at Menthosa Base Camp (MBC; Figures 1b and 2c). Menthosa is a tributary sub-basin of the Miyar. CEM DT-172 Temperature Humidity Hygrometer Data Logger was installed at Tingret and MBC to record air temperature and relative humidity at 30-minute intervals. Continuous temperature and humidity measurements were carried out between October 2015 and November 2019 (Figure 2d).

3.2. Satellite images

A total of 11 annual and six seasonal image pairs from multi-temporal Landsat missions (1992-2020) were used to quantify surface velocity in this study (Table 1), including six images from Landsat-5 Thematic Mapper (TM) between 1992–94 and 2009–11 and two scenes from Landsat-7 ETM+ (Enhanced Thematic Mapper Plus) for 2000 and 2002, and a series of Landsat-8 OLI (Operational Land Imager) images between 2013 and 2020 (Table 1; Supplementary Table S1). A complete Landsat scene (path 147 and row 37) covering the entire Miyar basin and adjacent regions was used for all surface velocity measurements (Supplementary Figure S1). All images were chosen during the ablation period (August-October) for annual velocity measurements, reducing seasonal snow cover and shadowing effects, except the 23 July 2013 image, where we could not obtain a cloud-free scene. Annual image pairs were chosen by limiting the presence of cloud cover and maximizing the similarity of the minimum sun angle and azimuth deviation between each two images. Seasonal velocities were measured between December

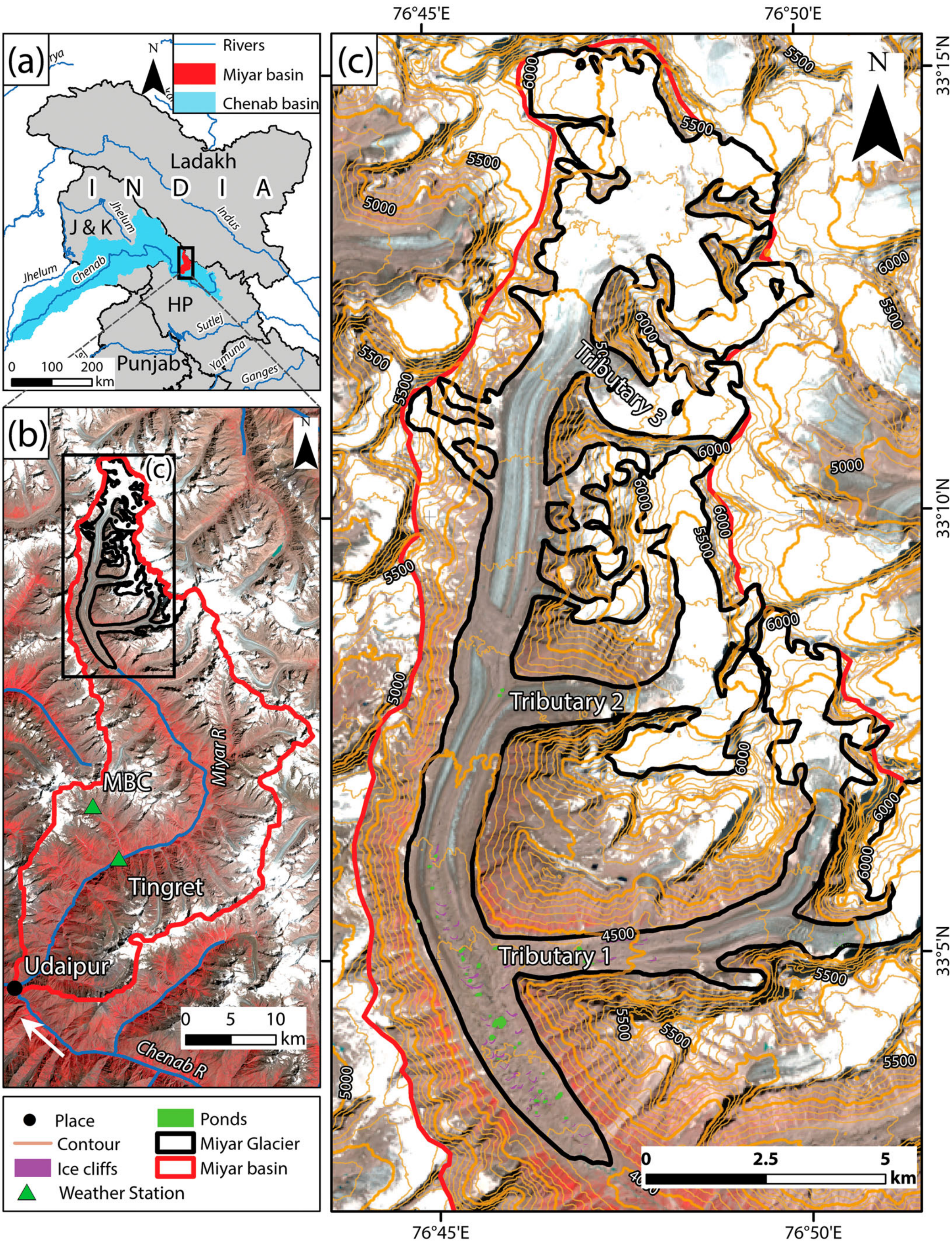

Figure 1. (a) Location of Miyar basin in the upper Chenab basin in the Himachal Pradesh, India. (b) Location of the Miyar Glacier in the Miyar basin. Green triangles show the location of the weather station at Menthosa Base Camp (MBC) and Tingret. (c) Landsat-8 RGB composite band (5-4-3) showing spatial distribution of debris-covered and clean ice and distribution of several ice cliffs and supraglacial ponds on Miyar Glacier. Contours are derived from ASTER GDEM and plotted at an interval of 100 m.

2018 and February 2020 with a temporal interval of 16 days from Landsat-8 OLI images (except the image pair of winter 2018; 32 days) to maintain the consistency of correlation among image pairs (Table 1; Supplementary Table S1). For comparison with other optical satellite images,

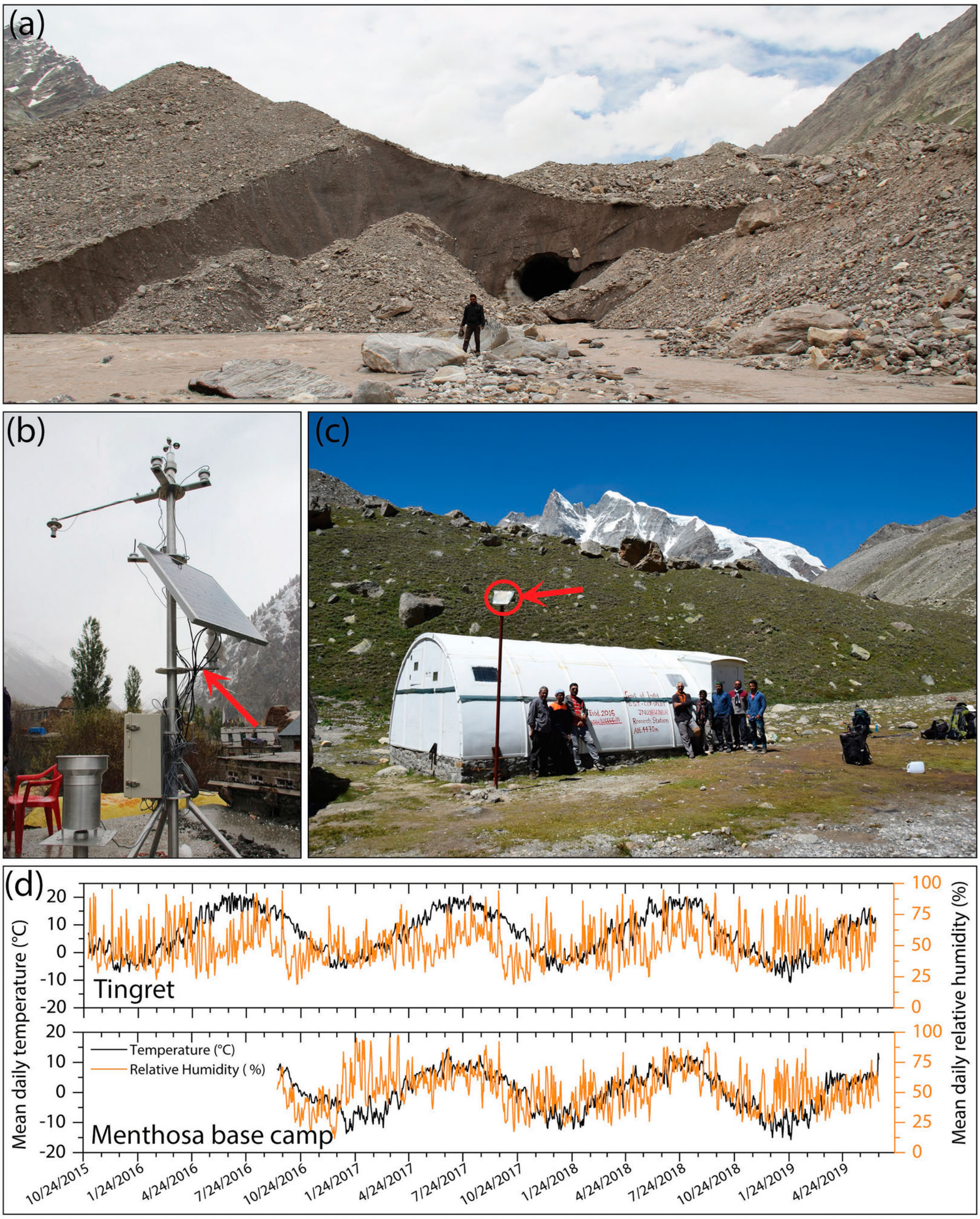

Figure 2. (a) Image of the snout of Miyar Glacier on 7 July 2013. (b) A weather station at Tingret. (c) The glaciological research station at Menthosa Base Camp (MBC) at 4470 m a.s.l. (d) On-site temperature and relative humidity measurements using CEM DT-172 Temperature Humidity Hygrometer Data Logger at Tingret and MBC during 2015-2019. At Tingret, the data logger was mounted on the weather station. Red arrows show the position of the data logger. The location of the weather station is shown in Figure 1b.

glacier velocity was derived from Sentinel-2A imagery for three time periods between 2016 and 2019 using band 8 (10 m spatial resolution). The difference between the acquisition dates of each two satellite image pairs is only seven days (Table 1).

Table 1. Satellite images used in this study and related uncertainty for each image pair.

Image pair	Satellite	Time [day]	Time [year]	Band/ Spatial resolution	Velocity in stable terrain (m)		Error assessment based on stable terrain (m)	
					Mean	STD	$SE = \frac{STD}{\sqrt{N_{off}}}$	$\sigma_{off} = \sqrt{SE^2 + MEAN^2}$
Annual velocity								
14Aug1992-17Aug1993	Landsat 5	368	1.01	Band 2/ 30 m	4.92	3.65	0.04	4.92
17Aug1993-20Aug1994		371	1.02		3.90	2.64	0.03	3.90
28Aug2000-02Aug2002	Landsat 7	704	1.93	Band 8/ 15 m	2.41	1.88	0.02	2.41
30Sept2009-17Sept2010	Landsat 5	352	0.96	Band 2/ 30 m	4.13	3.45	0.03	4.13
17Sept2010-22Oct2011		400	1.10		3.85	3.91	0.04	3.86
23July2013-28Sep2014	Landsat 8	432	1.18	Band 8/ 15 m	2.04	3.42	0.03	2.04
28Sept2014-15Sept2015		352	0.96		1.27	3.12	0.03	1.27
15Sept2015-03Oct2016		384	1.05		1.31	4.02	0.04	1.30
03Oct2016-30Sept2017		362	0.99		0.99	0.74	0.01	0.99
30Sept2017-22Aug2018		326	0.89		1.45	0.97	0.01	1.46
22Aug2018-10Sept2019		384	1.05		1.00	0.61	0.01	1.00
02Oct2016-07Oct2017	Sentinel 2A	370	1.02	Band 8/ 10 m	0.73	1.06	0.12	0.72
07Oct2017-20Sep2018		348	0.95		2.66	2.75	0.16	1.61
20Sep2018-10Sep2019		355	0.96		1.28	3.92	0.14	1.13
Seasonal Velocity								
26Nov2018-28Dec2018	Landsat 8	32	0.09	Band 8/ 15 m	0.07	0.08	0.00	0.07
18Mar2019-03Apr2019		16	0.04		0.25	0.35	0.00	0.25
05May2019-21May2019		16	0.04		0.42	0.85	0.01	0.42
08Jul2019-24Jul2019		16	0.04		1.00	1.88	0.02	1.00
12Oct2019-28Oct2019		16	0.04		0.07	0.08	0.01	0.07
01Feb2020-17Feb2020		16	0.04		0.19	0.26	0.00	0.19

Note: STD – Standard Deviation; SE- standard error; σ_{off}- uncertainty of stable terrain area.

3.3. Surface velocity extraction

3.3.1. Image cross-correlation

We calculated glacier surface velocities using the Co-registration of Optically Sensed Images and Correlation (COSI-Corr) technique, a free pixel tracking program for use with the ENVI software (Leprince et al. 2007). The algorithm available in COSI-Corr works on single-band grayscale images. In this study, the panchromatic band (PAN; band 8; 15 m; 0.50–0.66 µm for OLI and 0.52–0.9 µm for ETM+) for Landsat OLI and ETM+ and the green band (band 2; 30 m; 0.52–0.6 µm) for Landsat TM were processed (Table 1). The green band of Landsat TM was chosen as its wavelength is close to the PAN band of Landsat OLI and ETM+ images. We used the frequency correlation function to extract displacement with an initial and final window size of 64 and 32 pixels, respectively, step as 4 pixels, which resulted in a ground resolution of 60 m. The frequency mask threshold and robustness iteration were set as 0.9 and 2, respectively, to reduce the effect of noise on the correlation map. These threshold values were chosen based on previously published studies in the adjacent basins (Das and Sharma 2021). These parameter settings were used for the entire Landsat 7 and 8 PAN datasets to maintain the consistency of results. For Landsat TM green bands, we used a similar window size, but the step was reduced to 2 pixels. The details of surface velocity extractions are given in supplementary information. The flowchart of methodology for surface velocity extractions used in this study is presented in supplementary Figure S2.

Annual and seasonal velocity maps of the Miyar Glacier were obtained from 17 offset tracking image pairs between 1992-2020. The estimated velocity of each image pair was analyzed in terms of spatial and temporal scale during the observation periods. Seasonal velocities were grouped into four categories: (1) winter period: image pairs between December and February, (2) pre-melting: image pairs between March and May, (3) melting: June and August, and (4) post-melting: September to November. A robust continuous seasonal velocity dataset is challenging to produce due to changing snow compounds in the pixel-tracking method.

3.3.2. Post-processing

Rigorous post-processing was performed to remove the uncertainty related to temporal decorrelation noises, wavelength orbital error, satellite artifacts, attitude jitter distortions, and topography-dependent artifacts (Ding et al. 2016; Das and Sharma 2021). Erroneous measurements were masked out based on a low Signal-to-Noise-Ratio (SNR) value (< 0.9) to minimize decorrelation noise (see supplementary information section 1.3). Further, regions with cloud cover and shadow were manually checked, and resulting noises in East–West Direction (EWD) and North–South Direction (NSD) were removed using the replace/discard tool in COSI-Corr (i.e. NSD: −200 to 200 and ESD: −200 to 200). We used first-order polynomial fitting to reduce the wavelength orbital error using the detrend tool in COSI-Corr (Scherler et al. 2008; Ding et al. 2016; Das and Sharma 2021). A directional filter was applied to remove miscorrelated velocity vectors (Supplementary Figure S3). Finally, the velocity maps were smoothed using median filter 3*3 pixels (Copland et al. 2009; Millan et al. 2019).

3.3.3. Accuracy assessment

We estimated the image correlation error using the method suggested by Scherler et al. (2008): (1) a test of displacement in stable terrain (i.e. off-glacier areas), taking into account that off-glacier area should not move during the observation period; and (2) a test of the displacement direction based on streamlines along with the glacier flow. The error of the observed velocities in the off-glacier area was calculated based on the following formula (Berthier et al. 2003):

$$\sigma_{off} = \sqrt{SE^2 + MEAN^2} \tag{1}$$

where, σ_{off} is the error of the off-glacier velocity, $MEAN$ is the mean stack velocity of random points, and SE is the standard error of the mean velocity, which can be measured using the following equation:

$$SE = \frac{STD}{\sqrt{N_{off}}} \tag{2}$$

where STD is the standard deviation of the off-glacier area velocity and N_{off} is the number of measurements in the off-glacier area. In the present study, 10,000 random points were derived from the off-glacier area. Off-glacier displacements were evaluated based on the frequency distribution curve. We calculated the mean and standard deviation of off-glacier displacement for each annual and seasonal image pair (Supplementary Table S3). Glacier flow streamlines were manually digitized for the Miyar Glacier using Google Earth images. We overlaid the flow streamlines on the velocity vectors map to check the consistency and directions of the flow.

3.4. Other datasets and mapping

We used several other datasets (i.e. area change, snout migration, elevation change, ice and debris thickness, basal shear stress, surface morphology) to characterize the velocity pattern of the Miyar Glacier. Glacier terminus position was manually digitized from Landsat images for 1992, 2000, 2010, 2015, and 2019 periods and snout migrations were subsequently estimated. The debris-covered area was manually checked and corrected based on the higher-resolution images available in Google Earth and pan-sharpened Landsat-8 images of 2019. The elevation change map (2000-2020) of the Miyar Glacier was taken from Hugonnet et al. (2021). Debris thickness and sub-debris melt factors were taken from the study of Rounce et al. (2021). Ice thickness measurement was taken from the study of Farinotti et al. (2019). We calculated the basal shear stress using Eq. 3 (Cuffey and Paterson 2010):

$$\tau_b = H.\, f.\, p.\, g.\, sin\alpha_s \tag{3}$$

where τ_b is the basal shear stress (kilopascals = kpa), H is the ice thickness (m), f is the shape factor, p is the ice density, g is the acceleration due to gravity (9.8 ms^{-2}), and α_s is the ice surface slope. In this study, we assigned a constant ice density value of 917 km m^{-3}. The shape factor (f) ranges from 0.8–1.0 depending on the type, surface area, and location of a glacier. We used a shape factor value of 0.8 as reported for other Himalayan glaciers (Gantayat et al. 2014).

A glacial geomorphological map of targeted parts of the glacier was created to aid interpretation of the surface velocity, using high-resolution 3D optical images in Google Earth and 30 m global ASTER GDEM. To identify the relation between avalanche contribution and surface velocity, we mapped avalanche-fed zones of the Miyar Glacier (Supplementary Figure S4). The presence of snow avalanche cones and steep accumulation areas on hillslope above the glacier surface was considered to demarcate avalanche-fed glaciers. Crevasses and ogives on the glacier surface were manually identified and digitized (Supplementary Figure S4). Based on the crevasse area, the ice velocity of the crevasse zones was measured separately. Elevation-dependent ice distribution (i.e. hypsometry) and mean velocity at 25 m elevation bands were extracted from the ASTER DEM.

3.5. Climatic trend analysis

The Miyar basin does not have any climatic observatories. Long-term Asian Precipitation Highly Resolved Observational Data Integration Towards Evaluation (APHRODITE) gridded datasets were analyzed for the grid 33.25°N and 76.75°E to examine the historical climatic trend and seasonal fluctuation in temperature and precipitation (http://aphrodite.st.hirosaki-u.ac.jp/index.html). These datasets are primarily generated based on the data obtained from in situ measurements of rain gauge networks for Asia, including the Himalaya (Yatagai et al. 2012). Climatological long-term daily mean temperature (1961-2007) and precipitation (1951-2007) data are available at 0.25° horizontal resolution. The Mann-Kendall test was performed to analyze temperature and precipitation trends.

4. Results

4.1. Error analysis

We estimated the image correlation error from the analysis of calculated displacement over flat-lying, static off-glacier regions for the individual image pair (Table 1; Supplementary information). Any apparent displacements at these locations are due to misregistration and distortion produced during the orthorectification process. A linear curve fit was applied to identify the distribution pattern (Supplementary Figure S5). We found that off-glacier displacement is approximately normally distributed in east–west and north–south directions (Figure 3a–b). The spread of the distribution

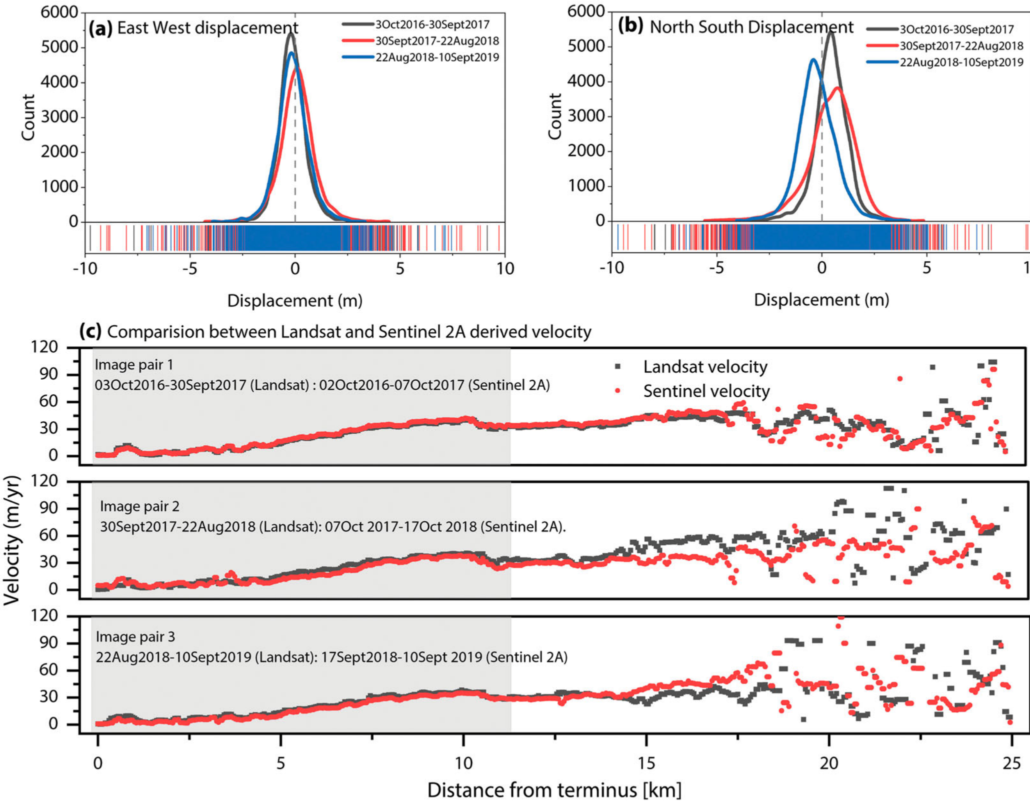

Figure 3. An example of frequency distribution of surface displacement over stable terrain areas in (a) East-west and (b) North-south direction for three different Landsat image pairs. The locations of the stable terrain are shown in Supplementary Figure S1. (c) Comparison between Landsat and Sentinel 2A derived surface velocity of Miyar Glacier for three different periods. Gray color sheds show the distribution of debris-cover from terminus to up-glacier zone.

provides an estimate of the random error in our image correlation. The resultant mean off-glacier displacement (and thus uncertainty in the velocity map) for each image pair ranges between 0.1–4.9 m, and the resultant standard deviation for each image pair ranges from 0.08–4.02 m (Table 1). The estimated uncertainty in the present study is in line with the previously reported studies in the Himalaya (Scherler et al. 2008; Satyabala 2016; Shukla and Garg 2020; Das and Sharma 2021). Sentinel-2A derived velocity showed a good coherence with Landsat-derived velocity (Figure 3c), except in the up-glacier area (over 20 km from snout), which is probably due to the frequent changes in snow conditions. In addition, glacier velocity vectors showed good consistency with flowlines, indicating the quality of the final velocity product.

4.2. Spatial velocity variations

4.2.1. Velocity variation along the glacier

The magnitude of surface velocity varies systematically along the length of this glacier (Figure 4). Velocity generally increases from the terminus to the upper glacier, although significant variations are visible (Figure 5a). In the lower part (up to 5 km from the terminus) of the glacier, the mean velocity (all observations during the studied period) is ~8.3 m/yr, with the lowest values present up to 3 km from the terminus of ~5.7 m/yr (Figure 5a). In the middle zone (between 5 and 20 km from the terminus along the central line), the mean velocity increases to 34.7 m/yr (nearly four times higher than the lower part). The upper part of the glacier (> 20 km from terminus)

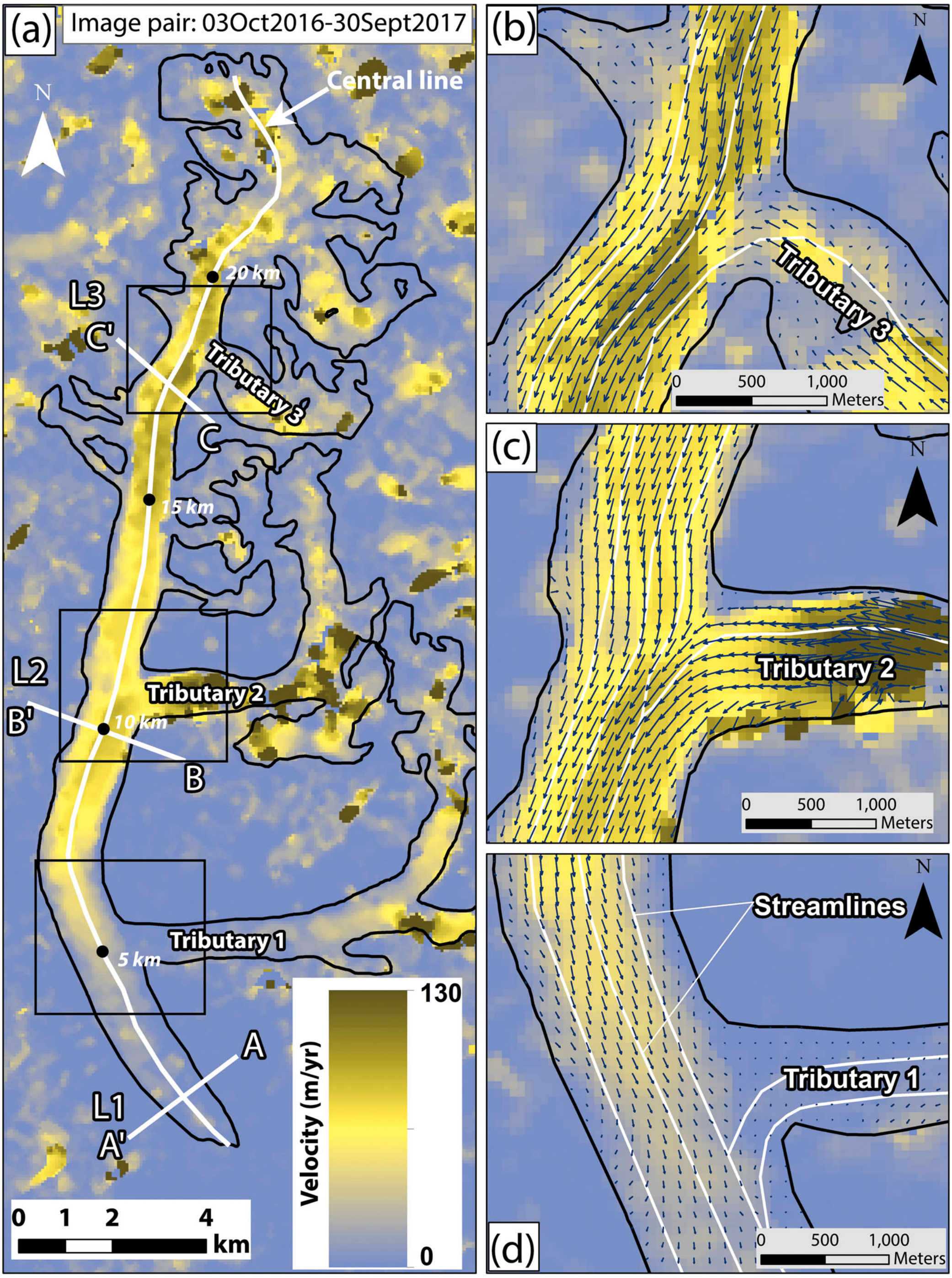

Figure 4. (a) Velocity map of Miyar Glacier derived from the cross-correlation of Landsat image (3 October 2016 and 30 September 2017). Central line and three across-glacier profiles are shown in white color. (b-d) Velocity maps from same image pair at the confluence of three tributaries. Arrows show the direction and magnitude of ice flow.

shows a mean velocity of ~35.5 m/yr along the flow line (Figure 5a). The greatest fluctuations are observed between 24 and 25 km from the terminus, with a peak velocity of > 100 m/yr during 2016–17 (Figures 4, 5a).

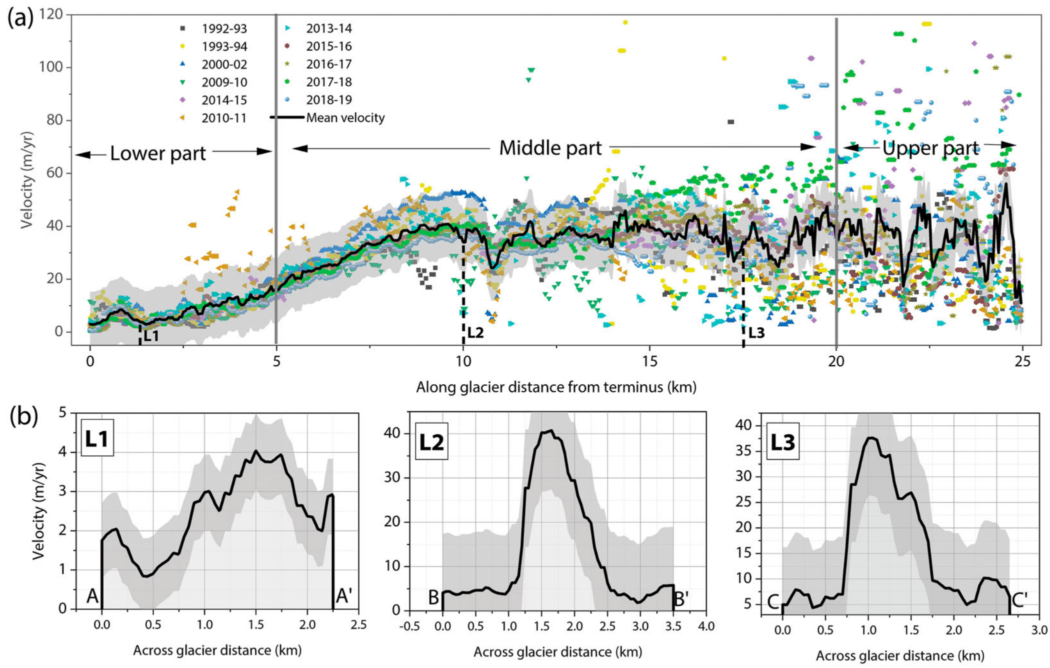

Figure 5. Spatial velocity variations of the Miyar Glacier. (a) Spatial velocity variation along the central flow line at 50 m intervals for all image pairs over the period 1992-2019. Black line shows the mean of all observations. (b) Across glacier mean velocity (average of all 11 observations between 1992 and 2019) for the three cross-sections shown in (a) from East (0 km) to West. Central line and across glacier profiles are shown in Figure 4a. Note that the vertical scale of the across glacier profiles is not the same. Gray shading on all panels shows the error estimation (± one standard deviation).

4.2.2. Velocity variation at the confluence of tributaries

Three active tributaries on the glacier's eastern margin show significant heterogeneity of surface velocity at the confluence with the trunk Miyar Glacier (Figure 4). The confluence of tributary 3 shows a mean velocity of ~20 m/yr on all image pairs, and the confluence of tributary 2 shows a mean velocity of ~40 m/yr (Figure 4(b and c)), with a maximum velocity of > 100 m/yr during 2016–17 (Figure 4b). In contrast, the mean velocity at the confluence of heavily debris-covered tributary 1 is < 5 m/yr (Figure 4d).

4.2.3. Velocity variation across the glacier

The across glacier profiles show an approximately parabolic shape, with a maximum velocity recorded in the central part and lower values towards the lateral margins (Figure 5b). In the debris-covered lower ablation zone, profile L1 shows a maximum mean velocity of 4 m/yr towards the western margin of the valley, while towards the eastern edge, the velocity is as low as ~1.5 m/yr (Figure 5b). For profiles L2 and L3, a maximum velocity of ~40 m/yr is observed in the middle of the glacier, but towards the lateral margins, the velocity is ~5 m/yr (Figure 5b).

4.3. Temporal velocity variations

4.3.1. Annual velocity variation

Miyar Glacier shows heterogeneous long-term inter-annual velocity variations during 1992–2019 (Figure 6). In the debris-covered lower zone (0-5 km from snout), velocity is very low (5 m/yr), with higher values (mean velocity of ~16.5 m/yr) observed only in 2010–11 (Figure 6b). In the middle zone, mean annual velocity varied from 29.3 m/yr during 2009–10 to 39.4 m/yr in 2018–

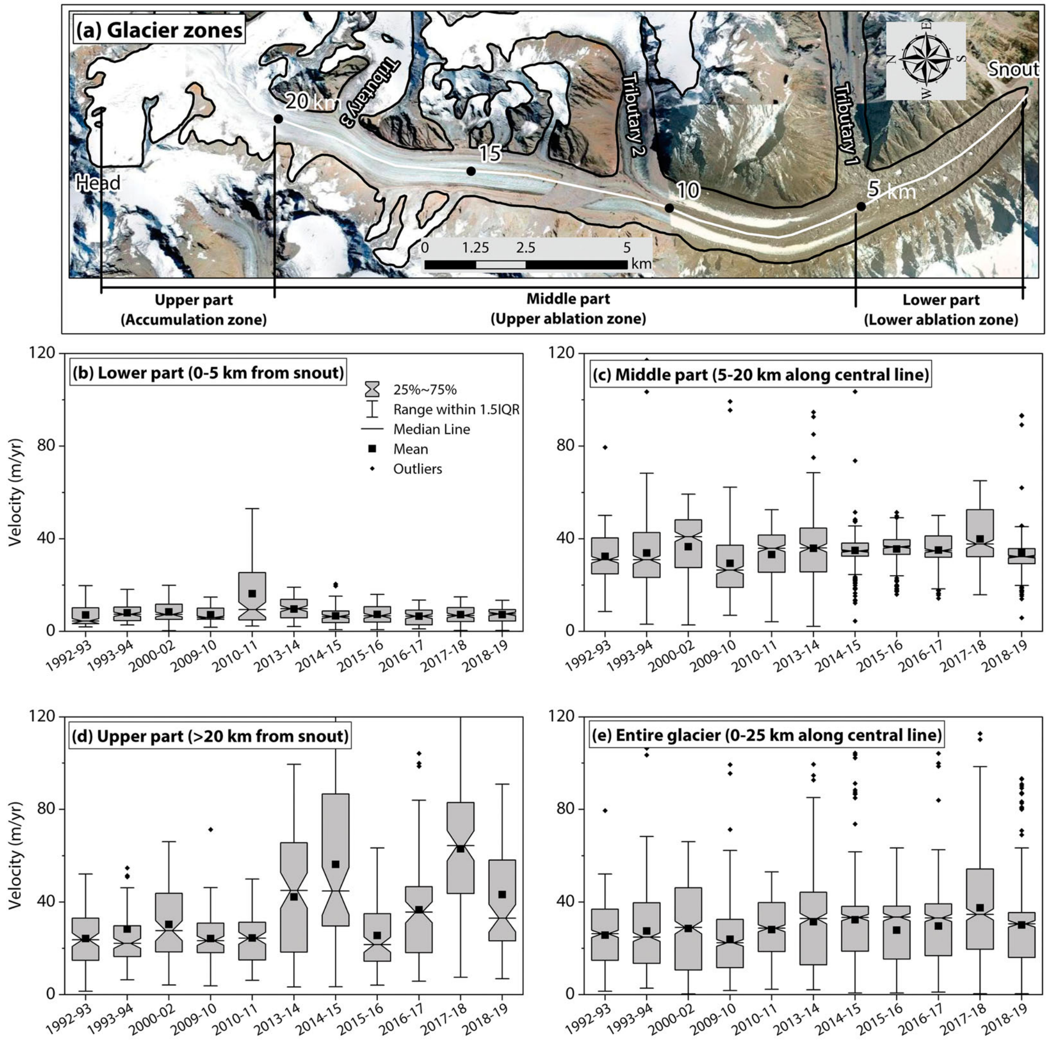

Figure 6. Zone-wise temporal velocity (annual) variations of Miyar Glacier between 1992 and 2019. (a) Division of glacier along the central flow line. Velocity variations in the (b) lower part (0-5 km from snout), (c) middle part (5-20 km along the flow line), (d) upper part (> 20 km from snout), and (e) entire profile (0-25 km).

19 (Figure 6c). In the upper part of the glacier (> 20 km from snout), mean annual velocity was more variable than in the lower glacier, with greater values shown later in the study period (2013-14, 2014-15, 2017-18, and 2018-19). For example, the mean annual velocity was 24.2 m/yr during 1992–93 compared to 62.6 m/yr during 2017–18 (Figure 6d). Overall mean velocity along the central flow line ranges between 20 and 40 m/yr during the observation period (Figure 6e).

4.3.2. Seasonal velocity variation

Figure 7a shows the seasonal change in velocity between December 2018 and February 2020. Velocity is low during winter (< 0.1 m/day during December-February) and increases during spring, reaching ~0.3 m/day in May. It reaches a maximum during summertime (~0.5 m/day during July) and decreases through the autumn (< 0.1 m/day in October) season (Figure 7(a and b)). These enhanced summer velocities are evident along the full glacier length, with all transerve velocity profiles showing a peak velocity during the melt season (Figure 7b). The greatest summer velocities

(> 1 m/yr) were observed in the upper ablation area and ~1 km down glacier of tributary 2 in July 2019 (Figure 7a).

4.4. Other parameters

The terminus of Miyar Glacier retreated by an average of 0.26 ± 0.04 km from 1992 to 2019, at an average annual rate of 0.009 ± 0.001 km/yr, resulting in a loss of area at the terminus of 0.25 ± 0.01 km^2 (Table 2). Terminus retreat was greater towards the western margin of the glacier (Figure 8a). The lowest rate of terminus retreat was observed from 1992–2000 (0.008 ± 0.003 km/yr) and the highest rate of terminus retreat from 2010–2015 (0.017 ± 0.007 km/yr). Debris-covered area increased by 5.03 ± 0.2 km^2 from 1992–2019 (0.18 ± 0.01 km^2/yr), from 19.18 ± 1.77 km^2 in 1992 to 24.21 ± 1.11 km^2 in 2019 (Table 2). The highest thinning rate was observed in the lower ablation zone (−1.31 m/yr) compared to the middle (−1.12 m/yr) and upper part (−0.61 m/yr) along the central flow line between 2000 and 2020 (Figure 8b).

The average modeled debris thickness is greatest (> 0.8 m) within 0–3 km and reduces to lowest (0.13 m) within 5–14 km along the central line (Figure 8c). Sub-debris melt increases as debris thickness decreases (Figure 8d). The average modeled ice thickness in the lower debris-covered zone (0-5 km from snout) is 228 m, increases to 302 m in the middle zone, and decreases to 250 m in the upper part along the central flow line, with the thickest ice up glacier of tributary 2 (Figure 8e). Ice thickness is greatest in the center of the valley and decreases towards valley edges. Calculated basal shear stress is proportionally related to ice thickness (Figure 8f).

The mean velocity of the glacier between October 2016 and September 2017 was compared to topographic characteristics, mapped on the glacier surface (Figure 9). The maximum velocity, and greatest variations in velocity occur at the transition zone between debris-covered and clean-ice (Figure 9a). Some of the highest velocities (>80 m/yr) are observed on tributary 2, where there is a notable change in surface gradient (break of slope) and an avalanche-contributing zone, compared to tributary 1 where velocities are consistently much lower (<5 m/yr), there is a gradual change in surface gradient, and no avalanche zones (Figure 9(b–d)).

4.5. Climatic trend

Long-term analysis of APHRODITE climatic data for the Miyar basin reveals that mean annual air temperature (1961-2015) generally increased over time (Table 3; Figure 10) with substantial annual variations and precipitation (1951-2007) shows no clear long-term trends but also demonstrates substantial annual fluctuations (Figure 10). The mean annual temperature (MAT) showed an increase of 1.72 °C (0.032°C per year) between 1961 and 2015 (Table 3). Except for the pre-melting season (March-May), all other seasons showed an increasing trend in temperature in this part of the Himalaya (Table 3; Supplementary Figure S6). The mean annual precipitation (MAP) shows higher values between 1980–1997 and particularly low values from 1997–2002 (Figure 10). The only significant monthly/seasonal trend was a decrease in precipitation during the pre-melting season (a maximum decrease of 45.08 mm in Mar-May from 1951-2007) (Table 3; Supplementary Figure S6).

5. Discussion

5.1. Heterogeneous spatial velocity patterns

Gravitational stresses of the ice drive glacier flow and, therefore, mainly depend on glacier thickness and slope (Nye 1952). Besides geometry (i.e. glacier size, length), several other topographic factors (i.e. hypsometry, elevation, surface gradient, aspect, curvature) also influence ice flow. Debris-

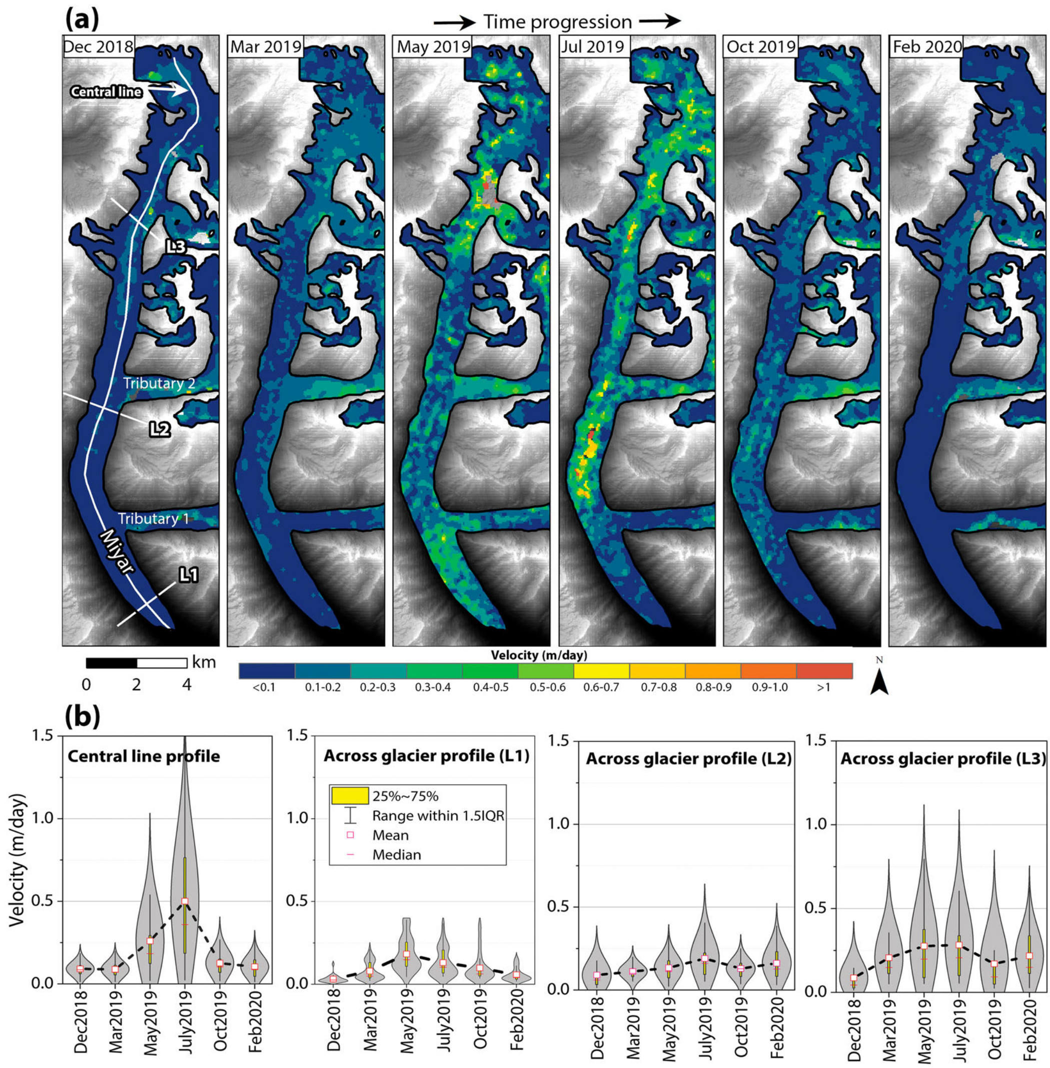

Figure 7. (a) Seasonal velocity evolution of Miyar Glacier during December 2018 – February 2020. (b) Seasonal velocity variations based on along (central line) and across (L1-L3) glacier profiles.

covered lower ablation zone of Miyar Glacier shows a near flat velocity curve (~5-10 m/yr) and is thus nearly stagnant (Figure 4d). In contrast, peak velocity is observed in the upper part of the glacier (~35 m/yr), leading to an asymmetrical velocity profile (Figure 5a), as has been observed for other glaciers in the Himalaya (Quincey et al. 2009; Satyabala 2016; Shukla and Garg 2020; Das and Sharma 2021). For example, Scherler et al. (2008) also observed an increasing glacier velocity with distance up glacier from the terminus of the debris-covered Gangotri Glacier. The hypsometric velocity distribution of Miyar Glacier shows that the transition zone between clean and debris-covered ice (4850-4950 m a.s.l, near the confluence of tributary 2) is highly active, with a mean velocity of ~34 m/yr (Figure 9a). A similar velocity pattern was observed for the Chhota Shigri glacier in the upper Chandra basin. Based on field measurements between 2003 and 2006, Wagnon et al. (2007) reported the greatest velocities of > 45 m/yr at 4850 m a.s.l in the upper ablation zone (4600-4850 m a.s.l.) compared to ~25 m/yr in the lower ablation area (~4400 m a.s.l). For Khumbu Glacier, greater surface velocities have also been observed in the upper clean-ice region (e.g. ~35-50 m/

Table 2. Changes in surface area, debris-covered area, and terminus position of Miyar Glacier between 1992 and 2019.

Years	Area (km^2)	DC ice (km^2)	Time periods	Terminus retreat		Loss in glacier area at the terminus		Debris cover increase	
				km	km/yr	km^2	km^2/yr	km^2	%
1992	84.59 ± 2.1	19.18 ± 1.77	1992–2019	0.268 ± 0.04	0.009 ± 0.001	0.25 ± 0.01	0.009	5.03 ± 2.0	26.24
2000	84.53 ± 1.5	20.96 ± 1.01	1992–2000	0.061 ± 0.03	0.007 ± 0.004	0.06 ± 0.01	0.007	1.78 ± 0.7	9.28
2010	84.46 ± 2.1	21.99 ± 1.96	2000–2010	0.096 ± 0.03	0.009 ± 0.003	0.08 ± 0.01	0.008	1.03 ± 0.4	4.91
2015	84.38 ± 1.5	23.62 ± 1.07	2010–2015	0.089 ± 0.03	0.017 ± 0.007	0.08 ± 0.01	0.016	1.63 ± 0.6	7.41
2019	84.33 ± 1.4	24.21 ± 1.11	2015–2019	0.055 ± 0.03	0.013 ± 0.008	0.05 ± 0.01	0.125	0.59 ± 0.2	2.49

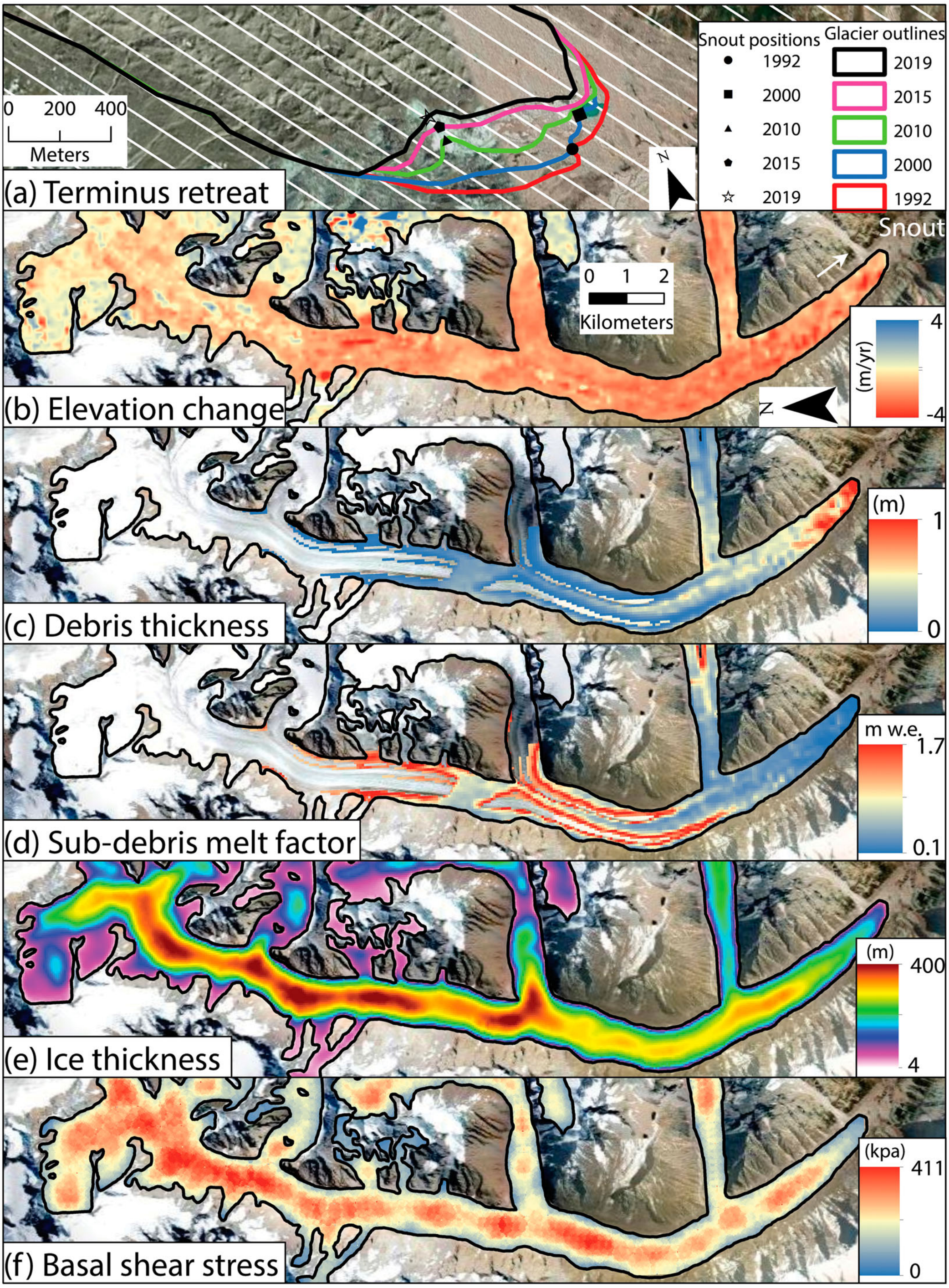

Figure 8. Multiparameter changes of Miyar Glacier. (a) Terminus change between 1992 and 2019. (b) Elevation change rate between 2000 and 2020 after Hugonnet et al. (2021). (c-d) Modeled debris thickness and sub-debris melt factor after Rounce et al. (2021). (e) Ice thickness after Farinotti et al. (2019). (f) Basal shear stress.

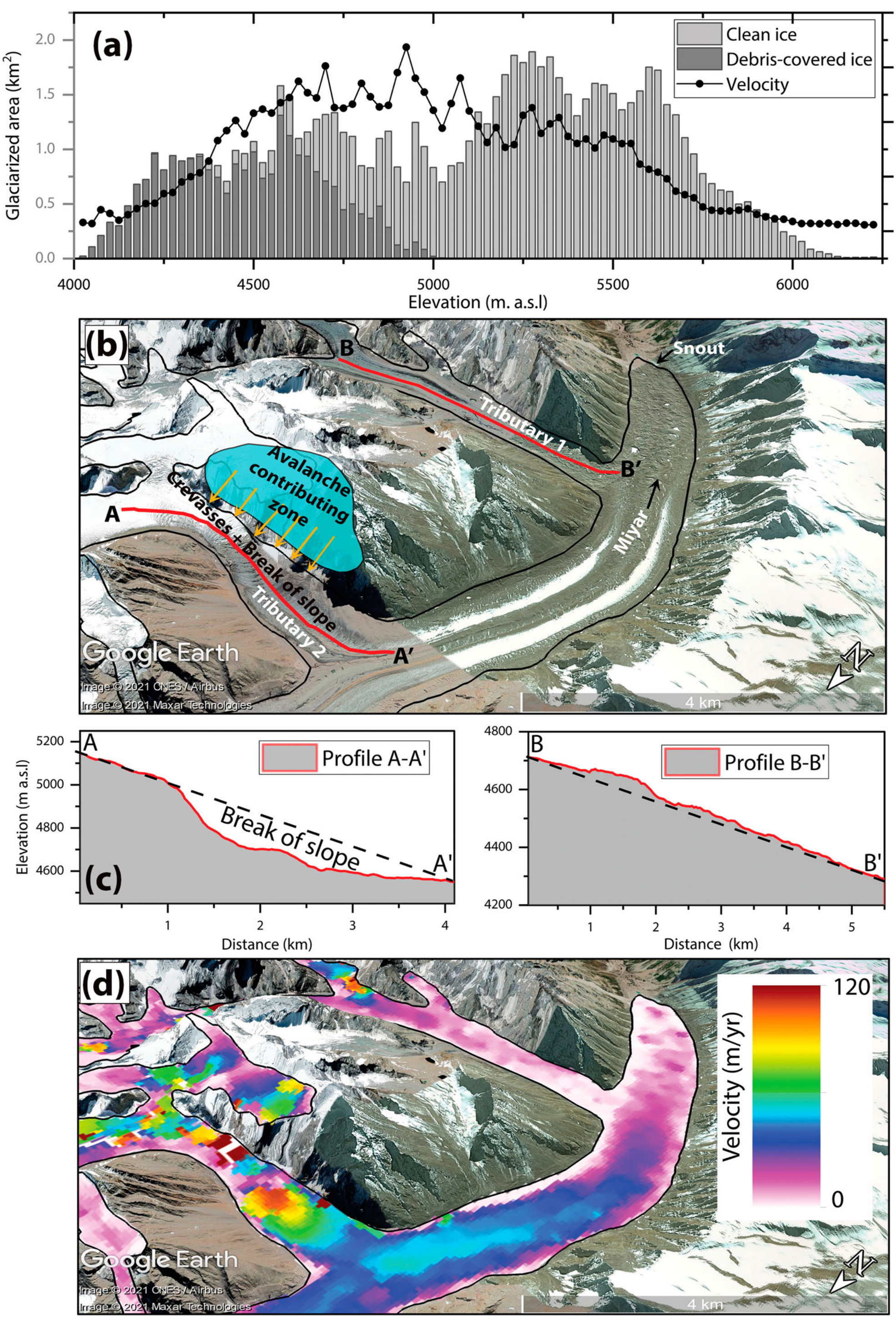

Figure 9. (a) Hypsometric velocity variation of Miyar Glacier derived for 25 m elevation bin from the cross-correlation of Landsat images (3 October 2016–30 September 2017). (b) Morphological characteristics of the lower ablation zone and two tributaries of Miyar Glacier. Avalanche-fed zones were manually mapped from Google Earth images using 3D view. (c) Elevation profile of two tributaries derived from ASTER GDEM. (d) Velocity variations from 03 Oct 2016–30 Sept 2017 plotted over the glacier surface.

Table 3. Monthly and seasonal Mann-Kendall test results of temperature (1961-2015) and precipitation (1951-2007) trend from APHRODITE data (grid: 33.25°N and 76.75°E) of the Miyar basin.

	Temperature			Precipitation		
Time series	Test Z	Significance level	Sen slope	Test Z	Significance level	Sen slope
January	2.352	*	0.019	−1.163		−0.220
February	2.744	**	0.033	0.805		0.167
March	2.367	*	0.035	−1.315		−0.348
April	2.570	*	0.030	−1.122		−0.209
May	3.514	***	0.045	−1.742		−0.251
June	2.323	*	0.017	1.384		0.151
July	5.532	***	0.032	−1.384		−0.320
August	5.517	***	0.032	0.764		0.154
September	4.370	***	0.030	−0.117		−0.029
October	4.109	***	0.027	−1.218		−0.105
November	5.038	***	0.035	0.255		0.011
December	4.399	***	0.027	−0.551		−0.057
Mean annual	6.272	***	0.032	−1.411		−0.105
Winter (Dec-Feb)	3.906	***	0.026	−0.489		−0.127
Pre-melting (Mar-May)	−3.659	***	−0.037	−2.196	*	−0.805
Summer (Jun-Aug)	5.256	***	0.028	−0.062		−0.031
Post-melting (Sep-Nov)	6.301	***	0.030	−0.516		−0.170

Note: Significance level: $P < 0.05$ *, $P < 0.01$ **, $P < 0.001$***.

yr near Everest base camp, compared to the debris-covered ablation zone (~5 m/yr) (Bolch et al. 2008), a pattern that has been observed across the Everest region (Quincey et al. 2009).

The higher velocity values measured in the transition zone from clean-ice to debris-covered of Miyar Glacier may be a consequence of surface gradient and ice thickness. Down glacier, debris-covered tributary 1 of Miyar Glacier has a surface gradient of < 0.5 degrees (Figure 9c) and a maximum mean velocity of ~6.5 m/yr along the flow line (Figure 9d). In contrast, tributary 2 has a break of slope along its flow path, giving a higher mean surface gradient of >30 degrees (Figure 9c) and a maximum mean velocity of ~62.5 m/yr within the same zone (Figure 9d). Steep slopes are known to encourage higher velocities (Quincey et al. 2009) and often result in extensional flow and the formation of crevasses, presence of which has been shown to directly correlate with surface velocity (Nye 1998; van der Veen 1999). The zone of crevasses on tributary 2 (Supplementary Figure S4) is highly active, with a maximum speed of > 80 m/yr compared to the other debris-covered parts of the Miyar Glacier (Figure 9d). The formation of ogives on tributary 2 (Supplementary Figure S4) suggests a surface gradient steep enough to create an ice fall zones of glaciers (King and Lewis 1961; Goodsell et al. 2002) that are known for very high velocities in a spatially limited area (Altena and Kääb 2020). In addition, the ice thickness of tributary 2 is expected to be greater than tributary 1 (Farinotti et al. 2019; Figure 8e), which would contribute a greater gravitational force on the ice and, therefore, higher surface velocity.

The debris-covered ablation zone of the Miyar Glacier was nearly stagnant during our studied period, with velocities < 5 m/yr (Figures 4a, 5, and 9d). We also observed a much smaller terminus retreat rate (9.9 ± 1.6 m/yr; Figure 8a) of Miyar glacier compared to other glaciers of similar morphology in the western Himalaya, e.g. Gangotri Glacier (19.9 ± 0.3 m/yr) (Bhambri et al. 2012) and Bara Shigri Glacier (22.5 ± 0.7 m/yr) (Chand et al. 2017). The area change rate of debris-covered glaciers is often less than that of clean-ice glaciers in the Himalayan region (Scherler et al. 2011; Dobhal et al. 2013), and the termini of some debris-covered glaciers, such as Khumbu Glacier, have not retreated from their terminal moraines, have extremely low surface velocities, and are thought to be dynamically detached from the active upper glacier (Miles et al. 2020). The insulating effects of the debris cover likely retard the frontal retreat, as debris layers greater than a few centimeters in thickness, as is the case for much of the lower ablation area of Miyar Glacier (Figure 8c), insulate the glacier surface from changes in air temperature (Östrem 1959). Thus, the termini of heavily debris-covered glaciers are often near stagnant in the Himalaya (Nuimura et al. 2011; Scherler et al. 2011b).

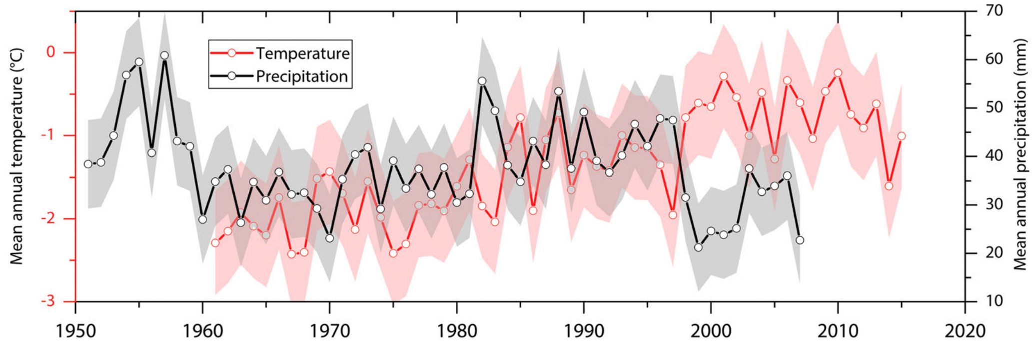

Figure 10. Long-term mean annual temperature (1961–2015) and precipitation (1951–2007) trend of the Miyar basin based on APHRODITE data (grid 33.25°N and 76.75°E).

5.2. Inter-annual and seasonal velocity variations

No studies have investigated high-resolution surface velocity variations of the Miyar Glacier on multi-temporal scales. Mean annual velocities of the glacier vary between 23.5 m/yr (1992) and 37.4 m/yr (2017-18) along the central flow line with significant inter-annual fluctuations, particularly in the upper glacier (> 20 km from the terminus) during the last decade (Figure 6d). The mean velocity of the Miyar Glacier during the last three decades (1992-2019) was ~29.6 m/yr, which is within the range of velocities measured for comparable glaciers in the upper Chandra basin (Wagnon et al. 2007; Shukla and Garg 2019; Yellala et al. 2019; Das and Sharma 2021; Patel et al. 2021) and in the wider Himalaya (Scherler et al. 2008; Quincey et al. 2009; Saraswat et al. 2013; Gantayat et al. 2014; Bhattacharya et al. 2016; Kraaijenbrink et al. 2016; Satyabala 2016; Shukla and Garg 2020). Based on in situ dGPS measurements, Patel et al. (2021) reported higher velocity for Samudra Tapu (64.3 ± 36.7 m/yr) and Sutri Dhaka (52.6 ± 17.3 m/yr) glaciers and comparatively slow movement in Gepang Gath (26.5 ± 12.9 m/yr) and Batal (6.2 ± 2.9 m/yr) glaciers in the Chandra basin. Differences in surface velocity within the basins could be due to heterogeneous topographic settings, the morphology of the debris-covered ice, contributions of tributary glaciers, and the role of local climatic fluctuations within catchments. In addition, the use of differential datasets (optical image, SAR, or field-based velocity measurements) could lead to heterogeneity in velocity estimation on spatial and temporal scales.

Miyar Glacier shows seasonal fluctuations in surface velocity, with 'summer speed-up' of ~67-80% compared to the winter, primarily in the mid-ablation area (Figure 7). Down glacier area of the confluence with tributary 2, part of an upper accumulation area, and the confluence with tributary 3 also reveals summer speed-up in seasonal velocities (Figure 7). Summer speed-up events have been observed on other glaciers across the Himalaya. For example, Satyabala (2016) reported an increase in summer velocity of ~57-126% compared to the winter velocities between 0 and 12.6 km from the terminus of the Gangotri Glacier. These recurring events showed peak summer speeds of 63.1 ± 5.4 m/yr in 1992, 66.6 ± 6.0 m/yr in 1999, 58.2 ± 4.5 m/yr in 2004, and 42.8 ± 4.2 m/yr in 2007, whereas winter speeds were relatively stable (~25-30 m/yr) during the same period. For 2009-10, Gantayat et al. (2014) also reported maximum summer velocities of ~61-85 m/yr during summer compared to minimum winter velocity of ~5-15 m/yr for Gangotri Glacier.

In the mid-ablation area, a substantial increase in surface velocity during the summer season may be due to enhanced basal sliding as a result of greater meltwater inputs to the subsurface drainage system from ablation and monsoon precipitation, as has been inferred for other glaciers in the Himalaya (Kraaijenbrink et al. 2016; Satyabala 2016) and European Alps (Hubbard and Nienow 1997; Mair 2002; Nienow et al. 2005; Vincent and Moreau 2016). The gradual reduction in velocity towards the early winter season implies a declining input into the subglacial system during the post-melting period, thus reducing the basal sliding. Similar results have been reported for the Gangotri Glacier in Uttarakhand Himalaya (Satyabala 2016) and Lirung Glacier in Nepal Himalaya (Kraaijenbrink et al. 2016). However, direct hydrological studies and field-based investigations, such as discharge measurements to analyze the sediment flux and evolution of the subglacial drainage system, are needed to ascertain the controls on these summer speed-up events.

The high velocities observed during the summer months in the upper accumulation area (above Tributary 3; Figures 1 and 7) are conversely unlikely to result from enhanced basal sliding. In high elevation areas of a glacier where mean annual air temperatures are low, ice is likely to be cold-based (Liu et al. 2009; Miles et al. 2018), restricting the presence of any subglacial hydrology (Irvine-Fynn et al. 2011; Miles et al. 2019) that might have an impact on ice velocity (Quincey et al. 2009; Tsutaki et al. 2018). However, enhanced observational velocities on Lirung Glacier were in the upper ablation area (Kraaijenbrink et al. 2016), as seen in this study for Miyar Glacier (Figure 7), which the authors attributed to a greater ice thickness creating greater driving stresses and basal sliding. The ice thickness of Miyar Glacier is the greatest just up glacier of the entire observed seasonal velocities, with high values of basal shear stress across this region (Figure 8(e and f)), which could also impact the glacier. Without knowledge of the glacier's thermal or hydrological regime, it is unknown whether the greater summer velocities in the upper ablation and accumulation area are due to enhanced driving stresses where the ice thickness is greater, or whether some form of basal sliding is occurring.

5.3. Potential climatic control on surface velocities

Besides geometric and topographic factors discussed earlier, temperature and precipitation variations are additional vital factors controlling ice flow velocities (Purdie et al. 2008; Scherler and Strecker 2012). Seasonal velocity variations are directly related to the seasonal fluctuations in temperature (Purdie et al. 2008), with warmer temperatures enhancing ablation and meltwater input into the subsurface drainage system. Our observations based on in situ measurements support this, with a minimum January mean monthly temperature of –3.2°C and a maximum July mean monthly air temperature of ~18°C at Tingret (Figure 2d).

Based on the climatic trend from the APHRODITE data, it might be argued that the higher mean annual surface velocities in recent years, particularly in the upper glacier, may reflect the influence of rising air temperature. Warming air temperatures increase ice ablation and meltwater production, which may percolate to the glacier bed and contribute to the increase rate of basal sliding. Increasing air temperatures have been shown to be amplified with elevation (Pepin et al. 2015), which could explain the increasing surface velocity trend in the upper part of the Miyar Glacier. However, in the present study, a lack of direct ground-based measurement of climatic parameters over the glacier itself largely hampers the assessment of the glacier's response to changes in temperature and precipitation.

6. Conclusion

This study presents the surface velocity variations of the debris-covered alpine valley type Miyar Glacier on a spatial and temporal scale during the last three decades (1992-2019). The mean velocity of the Miyar Glacier over this period was 29 m/yr, with the debris-covered tongue nearly stagnant (~5 m/yr) compared to the debris-free up glacier zone (> 60 m/yr). Glacier is most dynamic near the confluences of tributaries, particularly in the mid-ablation area, and where surface gradient shows a break in slope, giving maximum velocities of > 100 m/yr. The nearly stagnant debris-covered part of the Miyar Glacier is prone to higher surface lowering, associated with the growth of supraglacial ponds. Seasonal velocity shows an increase in summer surface velocity of ~67-80% (i.e. summer speed-up), interpreted as a result from basal sliding and enhanced driving stresses in areas of thicker ice. Increased basal sliding likely results from warmer summer air temperatures producing more ablation and thus meltwater input into the subsurface drainage system. Possible reasons for inter-annual fluctuations in surface velocity need further investigation, considering the overall rise in air temperature in the western Himalaya. Future studies should focus on the field-based ice velocity measurements to better understand debris-covered and clean ice dynamics independently. Further, microscale catchment basis datasets on climate are essential to evaluate the role of increasing temperature on the evolution of subglacial hydrological systems in the Himalaya.

Acknowledgment

The first author is thankful to the University Grant Commission, New Delhi (3090/ (NET–DEC.2014) for financial support during field visits in the Himalaya. The authors are grateful to Jawaharlal Nehru University for providing research facilities. Thanks to USGS for providing Landsat and Sentinel data at no cost. A special thanks to the entire COSI-Corr team for freely providing the software. We acknowledge the Department of Science and Technology (DST), Govt of India, for sponsoring the 'Himalayan Cryosphere: Science and Society' project (DST–CCP/SPLICE (IUCCCC)), for supporting field comparing and laboratory facilities. We thank Karin Ebert and two anonymous referees for their insightful suggestions, which considerably improved the earlier version of the manuscript.

Disclosure statement

No potential conflict of interest was reported by the author(s).

Data availability

Datasets generated in this study can be downloaded from http://doi.org/10.5281/zenodo.4898754

Notes on contributors

Suresh Das is a Ph.D. student in geography at Jawaharlal Nehru University, New Delhi. His research encompasses mapping and monitoring present and past cryosphere changes based on remote sensing, field mapping, and chronological methods. His contributions to this study is the conceptualization of the article, collection and analysis of remote sensing datasets, figure preparations, and writing the original draft.

Milap Chand Sharma is a professor of geomorphology at Jawaharlal Nehru University, New Delhi. His research focuses on field-based mapping and monitoring high-altitude Himalayan glaciers, reconstructing past glacial history using chronological methods. His contribution to this study is supervision and reviewing the draft.

Katie E Miles is an associate lecturer of glaciology and remote sensing at Aberystwyth University, United Kingdom. Her research focuses on the internal structure and subsurface hydrology of high-elevation debris-covered glaciers in the Himalaya through field-based measurements such as instrumented boreholes and dye tracing. Her contributions to this study are writing, reviewing, and figure preparations.

ORCID

Suresh Das http://orcid.org/0000-0003-4148-8551
Katie E. Miles http://orcid.org/0000-0003-2793-9766

References

Altena B, Kääb A. 2020. Ensemble matching of repeat satellite images applied to measure fast-changing ice flow, verified with mountain climber trajectories on Khumbu icefall, Mount Everest. J Glaciol. 66(260):905–915.

Azam MF, Wagnon P, Vincent C, Ramanathan A, Linda A, Singh VB. 2014. Reconstruction of the annual mass balance of Chhota Shigri glacier, western himalaya, India, since 1969. Ann Glaciol. 55(66):69–80.

Benn DI, Evans DJA. 2010. Glacier & glaciation. second Edi. London: Hodder Education.

Berthier E, Raup B, Scambos T. 2003. New velocity map and mass-balance estimate of mertz glacier, East Antarctica, derived from Landsat sequential imagery. J Glaciol. 49(167):503–511.

Bhambri R, Bolch T, Chaujar RK. 2012. Frontal recession of Gangotri Glacier, Garhwal Himalayas, from 1965 to 2006, measured through highresolution remote sensing data. Curr Sci. 102(3):489–494.

Bhambri R, Watson CS, Hewitt K, Haritashya UK, Kargel JS, Pratap Shahi A, Chand P, Kumar A, Verma A, Govil H. 2020. The hazardous 2017–2019 surge and river damming by Shispare glacier, Karakoram. Sci Rep. 10(1):1–14.

Bhattacharya A, Bolch T, Mukherjee K, Pieczonka T, Kropáček J, Buchroithner MF. 2016. Overall recession and mass budget of Gangotri Glacier, Garhwal Himalayas, from 1965 to 2015 using remote sensing data. J Glaciol. 62 (236):1115–1133.

Bhushan S, Syed TH, Arendt AA, Kulkarni AV. 2018. Assessing controls on mass budget and surface velocity variations of glaciers in western himalaya. Sci Rep. November 2017:1–11. doi:10.1038/s41598-018-27014-y.

Bindschadler R. 1983. The importance of pressurized subglacial water in separation and sliding at the glacier bed. J Glaciol. 29(101):3–19.

Bolch T, Buchroithner MF, Peters J, Baessler M, Bajracharya S. 2008. Identification of glacier motion and potentially dangerous glacial lakes in the Mt. Everest region/Nepal using spaceborne imagery. Nat Hazards Earth Syst Sci. 8 (6):1329–1340.

Chand P, Sharma MC, Bhambri R, Sangewar CV, Juyal N. 2017. Reconstructing the pattern of the Bara Shigri Glacier fluctuation since the end of the little Ice Age, Chandra valley, north-western himalaya. Prog Phys Geogr. 41 (5):643–675.

Copland L, Pope S, Bishop MP, Shroder JF, Clendon P, Bush A, Kamp U, Seong YB, Owen LA. 2009. Glacier velocities across the central Karakoram. Ann Glaciol. 50(52):41–49.

Cuffey KM, Paterson WS. 2010. The physics of glaciers. fourth edi. Oxford: Elsevier.

Das S, Sharma MC. 2021. Glacier surface velocities in the Jankar Chhu watershed, western himalaya, India: study using Landsat time series data (1992–2020). Remote Sens Appl Soc Environ. 24(August):100615. doi:10.1016/j.rsase.2021.100615.

Dehecq A, Gourmelen N, Gardner AS, Brun F, Goldberg D, Nienow PW, Berthier E, Vincent C, Wagnon P, Trouvé E. 2019. Twenty-first century glacier slowdown driven by mass loss in High Mountain Asia. Nat Geosci. 12(1):22–27. doi:10.1038/s41561-018-0271-9.

Dehecq A, Gourmelen N, Trouve E. 2015. Deriving large-scale glacier velocities from a complete satellite archive: Application to the Pamir-Karakoram-himalaya. Remote Sens Environ [Internet]. 162:55–66. doi:10.1016/j.rse.2015.01.031.

Deswal S, Sharma M, Saini R, Chand P, Juyal N, Singh I, Srivastava P, Ajai BI. 2017. Late holocene glacier dynamics in the Miyar basin, Lahaul Himalaya, India. Geosciences (Basel). 7(3):64. http://www.mdpi.com/2076-3263/7/3/64

Ding C, Feng G, Li Z, Shan X, Du Y, Wang H. 2016. Spatio-temporal error sources analysis and accuracy improvement in Landsat 8 image ground displacement measurements. Remote Sens. 8(11):1–22.

Dobhal DP, Mehta M, Srivastava D. 2013. Influence of debris cover on terminus retreat and mass changes of chorabari glacier, Garhwal region, central himalaya, India. J Glaciol. 59(217):961–971.

Fahnestock M, Scambos T, Moon T, Gardner A, Haran T, Klinger M. 2016. Rapid large-area mapping of ice flow using Landsat 8. Remote Sens Environ. 185:84–94. doi:10.1016/j.rse.2015.11.023.

Farinotti D, Huss M, Fürst JJ, Landmann J, Machguth H, Maussion F, Pandit A. 2019. A consensus estimate for the ice thickness distribution of all glaciers on earth. Nat Geosci. 12(3):168–173.

Gantayat P, Kulkarni AV, Srinivasan J. 2014. Estimation of ice thickness using surface velocities and slope: case study at Gangotri Glacier, India. J Glaciol. 60(220):277–282.

Gardner AS, Moholdt G, Scambos T, Fahnstock M, Ligtenberg S, Van Den Broeke M, Nilsson J. 2018. Increased west Antarctic and unchanged East Antarctic ice discharge over the last 7 years. Cryosphere. 12(2):521–547.

Garg PK, Garg S, Yousuf B, Shukla A, Kumar V, Mehta M. 2021. Stagnation of the pensilungpa glacier, western himalaya, India: causes and implications. J Glaciol. 1–15.

Garg PK, Shukla A, Tiwari RK, Jasrotia AS. 2017. Assessing the status of glaciers in part of the Chandra basin, Himachal himalaya: A multiparametric approach. Geomorphology. 284:99–114. doi:10.1016/j.geomorph.2016.10.022.

Glen JW. 1955. The creep of polycrystalline ice. Proc R Soc London Ser A Math Phys Sci. 228(1175):519–538.

Goodsell B, Hambrey MJ, Glasser NF. 2002. Formation of band ogives and associated structures at Bas glacier d'Arolla, valais, Switzerland. J Glaciol. 48(161):287–300.

Hubbard B, Nienow P. 1997. Alpine subglacial hydrology. Quat Sci Rev. 16(9):939–955.

Hugonnet R, McNabb R, Berthier E, Menounos B, Nuth C, Girod L, Farinotti D, Huss M, Dussaillant I, Brun F, Kääb A. 2021. Accelerated global glacier mass loss in the early twenty-first century. Nature. 592(7856):726–731. doi:10.1038/s41586-021-03436-z.

Irvine-Fynn TDL, Hodson AJ, Moorman BJ, Vatne G, Hubbard AL. 2011. Polythermal glacier hydrology: A review. Rev Geophys. 49(4):1–37.

Jiskoot H. 2011. Dynamics of glaciers. Encycl Earth Sci Ser. Part. 3(January 2011):245–256.

King CAM, Lewis W V. 1961. A tentative theory of ogive formation. J Glaciol. 3(29):912–939.

Kraaijenbrink P, Meijer SW, Shea JM, Pellicciotti F, De Jong SM, Immerzeel WW. 2016. Seasonal surface velocities of a Himalayan glacier derived by automated correlation of unmanned aerial vehicle imagery. Ann Glaciol. 57 (71):103–113.

Leprince S, Barbot S, Ayoub F, Avouac JP. 2007. Automatic, precise, ortho-rectification and coregistration for satellite image correlation, Application to ground deformation measurement. IEEE J Geosci Rem Sens. 45(6):1529–1558.

Liu Y, Hou S, Wang Y, Song L. 2009. Distribution of borehole temperature at four high-altitude alpine glaciers in Central Asia. J Mt Sci. 6(3):221–227.

Mair D. 2002. Influence of subglacial drainage system evolution on glacier surface motion: haut glacier d'Arolla, Switzerland. J Geophys Res. 107(B8):1–13.

Miles KE, Hubbard B, Irvine-Fynn TDL, Miles ES, Quincey DJ, Rowan AV. 2020. Hydrology of debris-covered glaciers in High Mountain Asia. Earth-Science Rev. 207:103212. doi:10.1016/j.earscirev.2020.103212.

Miles KE, Hubbard B, Quincey DJ, Miles ES, Irvine-Fynn TDL, Rowan AV. 2019. Surface and subsurface hydrology of debris-covered Khumbu Glacier, Nepal, revealed by dye tracing. Earth Planet Sci Lett. 513:176–186. doi:10.1016/j.epsl.2019.02.020.

Miles KE, Hubbard B, Quincey DJ, Miles ES, Sherpa TC, Rowan AV, Doyle SH. 2018. Polythermal structure of a Himalayan debris-covered glacier revealed by borehole thermometry. Sci Rep. 8(1):1–9. doi:10.1038/s41598-018-34327-5.

Millan R, Mouginot J, Rabatel A, Jeong S, Cusicanqui D, Derkacheva A, Chekki M. 2019. Mapping surface flow velocity of glaciers at regional scale using a multiple sensors approach. Remote Sens. 11(21):1–21.

Nienow PW, Hubbard AL, Hubbard BP, Chandler DM, Mair DWF, Sharp MJ, Willis IC. 2005. Hydrological controls on diurnal ice flow variability in valley glaciers. J Geophys Res Earth Surf. 110(4):1–11.

Nuimura T, Fujita K, Fukui K, Asahi K, Aryal R, Ageta Y. 2011. Temporal changes in elevation of the debris-covered ablation area of Khumbu Glacier in the Nepal Himalaya since 1978. Arctic, Antarct Alp Res. 43(2):246–255.

Nye J. 1998. The distribution of stress and velocity in glaciers and ice-sheets. Proc R Soc London. Series A. 239:113–133.

Nye JF. 1952. The mechanics of glacier flow. J Glaciol. 2(12):82–93.

Östrem G. 1959. Ice melting under a thin layer of moraine, and the existence of Ice cores in moraine ridges. Geogr Ann [Internet]. 41(4):228–230. https://www.tandfonline.com/doi/full/10.1080/20014422.1959.11907953

Patel LK, Sharma P, Fathima TN, Thamban M. 2018. Geospatial observations of topographical control over the glacier retreat, Miyar basin, western himalaya, India. Environ Earth Sci. 77(5):1–12. http://link.springer.com/10.1007/s12665-018-7379-5

Patel LK, Sharma P, Singh AT, Pratap B, Oulkar S, Thamban M. 2021. Spatial surface velocity pattern in the glaciers of Chandra basin, western himalaya. Geocarto Int. 0(0):1–18. doi:10.1080/10106049.2021.1920627.

Pepin N, Bradley RS, Diaz HF, Baraer M, Caceres EB, Forsythe N, Fowler H, Greenwood G, Hashmi MZ, Liu XD, et al. 2015. Elevation-dependent warming in mountain regions of the world. Nat Clim Chang. 5(5):424–430.

Prakash S, Sharma MC, Sreekesh S, Chand P, Pandey VK, Latief SU, Deswal S, Manna I, Das S, Mandal ST, Bahuguna IM. 2021. Decadal terminus position changes and ice thickness measurement of Menthosa glacier in Lahaul region of north-western himalaya. Geocarto Int. 0(0):1–20. doi:10.1080/10106049.2021.1939437.

Purdie HL, Brook MS, Fuller IC. 2008. Seasonal variation in ablation and surface velocity on a temperate maritime glacier : Fox glacier, New Zealand. Arctic, Antarct Alp Res. 40(1):140–147.

Quincey DJ, Braun M, Glasser NF, Bishop MP, Hewitt K, Luckman A. 2011. Karakoram glacier surge dynamics. Geophys Res Lett. 38(18):2–7.

Quincey DJ, Luckman A, Benn DI. 2009. Quantification of Everest region glacier velocities between 1992 and 2002, using satellite radar interferometry and feature tracking. J Glaciol. 55(192):596–606.

Rounce DR, Hock R, McNabb RW, Millan R, Sommer C, Braun MH, Malz P, Maussion F, Mouginot J, Seehaus TC, Shean DE. 2021. Distributed Global debris thickness estimates reveal debris significantly impacts glacier mass balance. Geophys Res Lett. 48(8):1–12.

Sahu R, Gupta RD. 2019. Spatiotemporal variation in surface velocity in Chandra basin glacier between 1999 and 2017 using landsat-7 and landsat-8 imagery. Geocarto Int [Internet]. 0(0):1–21. doi:10.1080/10106049.2019.1659423.

Saini R, Sharma MC, Deswal S, Barr ID, Pawan K, Parvendra K, Pankaj K, Chopra S. 2019. Glacio-archaeological evidence of permanent settlements within a glacier end moraine complex during 980-1840 AD: The Miyar basin, Lahaul Himalaya, India. Anthropocene. 26:100197. doi:10.1016/j.ancene.2019.100197.

Saraswat P, Syed TH, Famiglietti JS, Fielding EJ, Crippen R, Gupta N. 2013. Recent changes in the snout position and surface velocity of Gangotri glacier observed from space. Int J Remote Sens. 34(24):8653–8668. doi:10.1080/01431161.2013.845923.

Satyabala SP. 2016. Spatiotemporal variations in surface velocity of the Gangotri glacier, Garhwal Himalaya, India: study using synthetic aperture radar data. Remote Sens Environ. 181:151–161. doi:10.1016/j.rse.2016.03.042.

Scambos TA, Fahnestock M, Moon T, Gardner AS, Klinger M. 2016. Global Land Ice Velocity Extraction from Landsat 8 (GoLIVE).

Scherler D, Bookhagen B, Strecker MR. 2011. Spatially variable response of Himalayan glaciers to climate change affected by debris cover. Nat Geosci. 4(3):156–159. http://www.nature.com/doifinder/10.1038/ngeo1068

Scherler D, Leprince S, Strecker MR. 2008. Glacier-surface velocities in alpine terrain from optical satellite imagery-Accuracy improvement and quality assessment. Remote Sens Environ. 112(10):3806–3819.

Scherler D, Strecker MR. 2012. Large surface velocity fluctuations of biafo glacier, central Karakoram, at high spatial and temporal resolution from optical satellite images. J Glaciol. 58(209):569–580.

Shugar DH, Burr A, Haritashya UK, Kargel JS, Watson CS, Kennedy MC, Bevington AR, Betts RA, Harrison S, Strattman K. 2020. Rapid worldwide growth of glacial lakes since 1990. Nat Clim Chang. 10(10):939–945. doi:10.1038/s41558-020-0855-4.

Shukla A, Garg PK. 2019. Evolution of a debris-covered glacier in the western Himalaya during the last four decades (1971–2016): A multiparametric assessment using remote sensing and field observations. Geomorphology. 341:1–14. doi:10.1016/j.geomorph.2019.05.009.

Shukla A, Garg PK. 2020. Spatio-temporal trends in the surface ice velocities of the central Himalayan glaciers, India. Glob Planet Change. 190(March):103187. doi:10.1016/j.gloplacha.2020.103187.

Steiner JF, Kraaijenbrink PDA, Immerzeel WW. 2021. Distributed melt on a debris-covered glacier: field observations and melt modeling on the Lirung Glacier in the himalaya. Front Earth Sci. 9(July):1–21.

Thompson S, Benn DI, Mertes J, Luckman A. 2016. Stagnation and mass loss on a Himalayan debris-covered glacier: processes, patterns and rates. J Glaciol. 62(233):467–485.

Tsutaki S, Fujita K, Nuimura T, Sakai A, Sugiyama S, Komori J, Tshering P. 2018. Contrasting thinning patterns between lake- and land-terminating glaciers in the Bhutan himalaya. Cryosph. 2010:1–29.

van der Veen CJ. 1999. Crevasses on glaciers. Polar Geogr. 23(3):213–245.

Vincent C, Moreau L. 2016. Sliding velocity fluctuations and subglacial hydrology over the last two decades on argentière glacier, mont blanc area. J Glaciol. 62(235):805–815.

Wagnon P, Linda A, Arnaud Y, Kumar R, Sharma P, Vincent C, Pottakkal JG, Berthier E, Ramanathan A, Hasnain SI, Chevallier P. 2007. Four years of mass balance on Chhota Shigri glacier, Himachal Pradesh, India, a new benchmark glacier in the western himalaya. J Glaciol. 53(183):603–611.

Wagnon P, Vincent C, Arnaud Y, Berthier E, Vuillermoz E, Gruber S, Ménégoz M, Gilbert A, Dumont M, Shea JM, et al. 2013. Seasonal and annual mass balances of mera and pokalde glaciers (Nepal Himalaya) since 2007. Cryosphere. 7(6):1769–1786.

Watson CS, Quincey D. 2015. Glacier movement. In: Cook S.J., Clarke L.E., Nield J.M., editor. Geomorphological techniques (online edition). London, UK: British Society for Geomorphology; p. 1–13. ISSN: 2047-0371.

Weertman J. 1957. On the sliding of glaciers. J Glaciol. 3(21):33–38.

Westoby MJ, Glasser NF, Brasington J, Hambrey MJ, Quincey DJ, Reynolds JM. 2014. Modelling outburst floods from moraine-dammed glacial lakes. Earth-Science Rev. 134:137–159. doi:10.1016/j.earscirev.2014.03.009.

Yatagai A, Kamiguchi K, Arakawa O, Hamada A, Yasutomi N, Kitoh A. 2012. Aphrodite constructing a long-term daily gridded precipitation dataset for Asia based on a dense network of rain gauges. Bull Am Meteorol Soc. 93 (9):1401–1415.

Yellala A, Kumar V, Høgda KA. 2019. Bara Shigri and Chhota Shigri glacier velocity estimation in western Himalaya using sentinel-1 SAR data. Int J Remote Sens. 40(15):5861–5874. doi:10.1080/01431161.2019.1584685.